DRAFT VERSION, NOVEMBER 19, 2012
Preprint typeset using LaTeX style emulateapj v. 03/07/07

GRAVITATIONAL DRAG ON A POINT MASS IN HYPERSONIC MOTION WITHIN A GAUSSIAN DISK

J. CANTÓ[1], A. ESQUIVEL[2], F. J. SÁNCHEZ-SALCEDO[1], A. C. RAGA[2]
[1]Instituto de Astronomía, Universidad Nacional Autónoma de México, Ap. 70-468, 04510 D.F., México
[2]Instituto de Ciencias Nucleares, Universidad Nacional Autónoma de México, Apartado Postal 70-543, 04510 México D.F., México

Draft version, November 19, 2012

ABSTRACT

We develop an analytical model for the accretion and gravitational drag on a point mass that moves hypersonically in the midplane of a gaseous disk with a Gaussian vertical density stratification. Such a model is of interest for studying the interaction between a planet and a protoplanetary disk, as well as the dynamical decay of massive black holes in galactic nuclei. The model considers that the flow is ballistic, and gives fully analytical expressions for both the accretion rate onto the point mass, and the gravitational drag it suffers. The expressions are further simplified by taking the limits of a thick, and of a thin disk. The results for the thick disk reduce correctly to those for a uniform density environment (Cantó et al. 2011). We find that for a thin disk (small vertical scaleheight compared to the gravitational radius) the accretion rate is proportional to the mass of the moving object and to the surface density of the disk, while the drag force is independent of the velocity of the object. The gravitational deceleration of the hypersonic perturber in a thin disk was found to be independent of its parameters (i.e. mass or velocity) and depends only on the surface mass density of the disk. The predictions of the model are compared to the results of three-dimensional hydrodynamical simulations, with a reasonable agreement.

Subject headings: black hole physics — hydrodynamics — stars: formation — ISM: clouds — ISM: kinematics and dynamics

1. INTRODUCTION

A gravitational point-like particle moving in a background gas can capture ambient matter. In addition, the particle may experience a drag due to the interaction with the wake that it induces in the medium. Both accretion and dynamical friction are ubiquitous phenomena in astrophysics, from protostars embedded in molecular clumps to supermassive black holes at the center of galaxies (e.g., Sánchez-Salcedo 2012).

Bondi, Hoyle and Lyttleton (Hoyle & Lyttleton 1939, 1940a, 1940b, 1940c; Bondi 1952) treated the problem by assuming a point mass moving at constant speed within a uniform gaseous media. By neglecting the pressure of gas except on the downstream axis, Bondi & Hoyle (1944) derived a formula that gives the accretion rate as a function of the Mach number for highly supersonic flows. Later on, Bondi (1952) suggested an approximate formula for any Mach number. Some authors have used Bondi's formula to account for the initial mass function of stars as a competition for gas accretion by protostars (Bonnell et al. 2001a,b; Klessen & Burkert 2000, 2001) and to estimate the rate at which supermassive black holes accrete mass (e.g., Di Matteo et al. 2001).

The loss of momentum of the object relative to the cloud due to its gravitational interaction with its wake was also envisaged in Bondi & Hoyle (1944) using their line-accretion model. Traditionally, however, the gravitational drag force has been derived by calculating the density structure of the wake in linear perturbation theory (Dokuchaev 1964; Ruderman & Spiegel 1971; Just & Kegel 1990; Ostriker 1999; Kim & Kim 2007; Sánchez-Salcedo 2009, 2012; Namouni 2010). In this approach, a minimum radius $r_{\rm min}$ must be introduced because the linear approximation is not valid close enough to the perturber. Recently, Cantó et al. (2011) were able to calculate the contribution of the nonlinear inner part of the wake to the gravitational drag on hypersonic perturbers by using the ballistic orbit theory.

All the abovementioned papers have considered that the surrounding gaseous medium is initially uniform, of constant density ρ_0. In this case and for a polytropic gas, the accretion rate and the gravitational drag are largely characterized by the Mach number. Because of the assumption that the medium is infinite, the gravitational drag on supersonic bodies increases logarithmically in time (e.g., Ostriker 1999). In real life, however, systems are finite in size. Whilst the problem of the dynamical friction in non-homogeneous (usually flattened) collisionless systems has received considerable attention (eg., Binney 1977; Tremaine & Weinberg 1984; Maoz E. 1993; Colpi et al. 1999; Just & Peñarrubia 2005), less studied is the case for gaseous systems. Sánchez-Salcedo & Brandenbrug (2001) simulated the orbital decay of a satellite in orbit around a Plummer sphere of gas and found that the "local approximation", that is estimating the drag force at the present location of the perturber as if the medium were homogeneous (but taking appropriately the Coulomb logarithm) is very successful.

In this paper we study the gravitational drag on a body moving in the midplane of a vertically-stratified gaseous disk. It has been recently noted that the dynamical friction in a gaseous slab could be useful to describe the interaction between a planet in an eccentric orbit and the protoplanetary disk (Muto et al. 2011). These authors argue that the standard analysis of the interaction between a planet and the disk, which assumes that the planet is corotating with the disk, is not valid when the planet eccentricity exceeds the disk aspect ratio. Instead, for moderate and large eccentricities, they suggest it is more convenient to use the dynamical friction formula. They derived the dynamical friction force felt by a perturber moving in an infinitesimally thin disk of constant

Electronic address: esquivel@nucleares.una.mx; jsanchez@astro.unam.mx; raga@nucleares.unam.mx

surface density and calculated the migration and eccentricity damping timescales. When the dynamical friction formula is applied to planets with moderate eccentricities, the migration and eccentricity damping timescales are in agreement with those found in previous works.

Gaseous dynamical friction is also relevant to study the disk-planet interaction in highly inclined systems. Rein (2012) computed the time-scales associated with migration and inclination damping of planets due to dynamical friction with the protoplanetary disk in the linear approximation and compared the results with simulations. In order to model the gravitational interaction, he uses a large softening radius, so that their simulations also lie in the linear regime as well. This is justified as long as the physical radius of the planet r_p is much larger than its accretion radius ($R_A \equiv 2GM/v^2$, where v is the velocity of planet relative to the gas in the disk). For a hot Jupiter with a mass of 100 Earth masses and a size of 10 Earth radii moving on an inclined circular orbit around a star, the condition $r_p > R_A$ implies inclinations between the orbit of the planet and the plane of the disk larger than $\sim 71^\circ$. In the present work, we are interested in modelling the nonlinear contribution of the gravitational wake to the drag force on an accreting point-mass moving in non-inclined orbits.

A second area of application is in the orbital decay of massive black holes residing in galactic nuclei. The formation of massive black hole binaries following galaxy mergers is a natural consequence of the hierarchical scenario (e.g., Begelman et al. 1980). The gravitational torque due to dynamical friction with an accretion disk formed by gas that was funnelled to the central 100 pc, is expected to be responsible for the in-spiral toward the center of the merger remnant down to pc separations (Escala et al. 2005; Dotti et al. 2007; Cuadra et al. 2009; Khan et al. 2011; Preto et al. 2011; Roedig et al. 2012). Recently, Nixon et al. (2011a,b) showed that the binary orbital angular momentum and energy are more efficiently removed in a retrograde accretion disk than they are in a prograde accretion disk because there are no orbital resonances between the binary and the disk. Since there is no compelling reason to assume that the binary and the disk rotation are initially parallel, it is quite possible that retrograde disks strongly promote coalescence of the black hole binary.

So far, most of the semi-analytical models aimed to study the assembly of black holes use a prescription for the dynamical drag (e.g., Tanaka & Haiman 2009). Given the importance of having analytical formulae to be applied for planets or black holes in eccentric or counter-rotating orbits, the strategy in our paper is to provide analytical estimates for the gravitational drag on an accreting object embedded in a three-dimensional disk of gas and to check its validity through numerical simulations. We will focus on highly supersonic perturbers. For instance, if a perturber is in orbit within a disk whose aspect ratio is constant with radius, the relative velocity between the perturber and its surroundings will be always supersonic if its eccentricity exceeds the disk aspect ratio (see, for instance, Muto et al. 2011). Moreover, it is clear that perturbers in retrograde disks also move supersonically, even if the orbit is circular. We will concentrate on a Gaussian vertical profile, but the method is general and can be applied for any decaying profile.

2. THE FREE STREAMING MODEL

We consider the problem of a point mass M moving hypersonically at velocity v_0 in a stratified, gaseous medium. As a result of the gravitational pull produced by M the otherwise straight trajectory of a fluid parcel is bent, and a wake behind the perturber is formed (see the top panel of Figure 1). In the hypersonic limit, the solution for the trajectory of a fluid parcel (streamline) can be obtained neglecting the pressure force and considering that the motion is ballistic. By hypersonic we mean that the dynamical pressure is much larger than the thermal pressure, i.e. $v_0^2 \gg c_s^2$, where c_s is the sound speed, so that the Mach number $\mathcal{M}$ satisfies $\mathcal{M}^2 \gg 1$. The case of a uniform environment was treated in Cantó et al. (2011) and a comparison of the analytic model and a numerical simulation was presented.

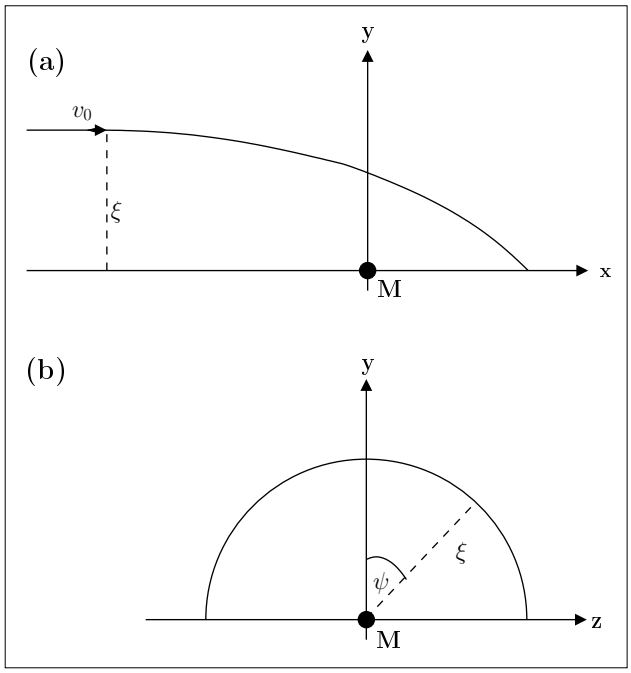

FIG. 1.— Schematic diagram of the geometry and reference frame used in the model (the mass M is at rest). Far from the source a fluid parcel has a velocity v_0 (parallel to the x-axis), and an impact parameter ξ, but as it approaches the point mass its trajectory is deflected as illustrated in panel (a). In panel (b) the angle ψ is shown in a view perpendicular to the relative motion of M with respect to the environment.

In the present paper we consider that the point mass moves in the mid-plane of a plane-parallel structure, whose density decays in the vertical direction y. For illustration, we will assume a rather realistic Gaussian vertical density profile of the form

$$\rho\left(y\right) = \rho_0\, \mathrm{e}^{-y^2/h^2} = \rho_0\, \mathrm{e}^{-(\xi\cos\psi)^2/h^2}, \qquad (1)$$

where ρ_0 is the midplane density, h is the scaleheight, ξ is the fluid parcel impact parameter, and the angle ψ is measured from the y-axis (see Figure 1). We adopt the same reference frame as in Cantó et al. (2011), in which the point mass M is at rest. In this reference frame, the motion can be modeled as a streaming environment with a constant velocity v_0 far upstream of the source. The undisturbed, streaming velocity v_0 lies in the positive x direction.

In a hypersonic regime, the trajectories of the parcels, subject to the gravitational field of M, have initially positive energy (per unit mass) $E = v_o^2/2$ and therefore they are hyperbolic. The velocity of each parcel of gas is the same as in Cantó et al. (2011), that is, the solution of the hyperbolic trajectory after imposing the upstream v_0 boundary condition and requiring angular momentum conservation along the streamlines. Our model assumes that when the fluid encounters the x-axis, the other velocity components (v_y and v_z) are

thermalized at a shock, and the corresponding energy is immediately radiated away. This condition results in a decrease of the kinetic energy from $E_0 = v_0^2/2$ at $x \to -\infty$ to

$$E_{\rm tot} = \frac{v_0^2}{2}\left[1 - \left(\frac{2\xi_0}{\xi}\right)^2\right], \quad (2)$$

where ξ_0 is the gravitational radius (Bisnovatyi-Kogan et al. 1979; Cantó et al. 2011), defined as

$$\xi_0 \equiv \frac{GM}{v_0^2}\,. \quad (3)$$

From equation (2) it is clear that all the material with an impact parameter $\xi \leq 2\xi_0$ after the shock has a negative energy and thus remains gravitationally bound (i.e., it will eventually be accreted onto the point mass).

From equation (2) we can also see that the material that is gravitationally unbound when entering the wake will flow away along the x-axis reaching infinity with a velocity

$$v_\infty = v_0\left[1 - \left(\frac{2\xi_0}{\xi}\right)^2\right]^{1/2}. \quad (4)$$

2.1. *The mass accretion rate and the gravitational drag*

The accretion rate can be calculated by integrating over all the material intercepted by a cylinder with an impact parameter up to $2\xi_0$:

$$\dot{M}_{\rm acc} = \int_0^{2\xi_0} 2\pi\,\bar{\rho}(\xi)\,v_0\,\xi\,{\rm d}\xi, \quad (5)$$

where $\bar{\rho}(\xi)$ is the ψ-averaged density for a given impact parameter ξ. This average is obtained as:

$$\bar{\rho}\,(\xi) = \frac{1}{2\pi}\int_0^{2\pi}\rho\,(\xi,\psi)\;{\rm d}\psi = \rho_0\,{\rm e}^{-\xi^2/2h^2}{\rm I}_0\left(\frac{\xi^2}{2h^2}\right), \quad (6)$$

where ${\rm I_n}(x)$ is the modified Bessel function of the first kind. Substituting equation (6) into equation (5) and performing the integral one obtains:

$$\dot{M}_{\rm acc} = 4\pi\,\rho_0\,v_0\,\xi_0^2\,{\rm e}^{-2\xi_0^2/h^2}\left[{\rm I}_0\left(\frac{2\xi_0^2}{h^2}\right) + {\rm I}_1\left(\frac{2\xi_0^2}{h^2}\right)\right]. \quad (7)$$

The drag force felt by the point mass can be calculated considering the net loss of momentum flux along the x-direction. Material coming into the system from $x \to -\infty$ carries a ρv_0 momentum flux, while material leaving the system at $x \to \infty$ (fluid parcels with $\xi \geq 2\xi_0$) takes a ρv_∞ momentum flux, thus the drag can be obtained as

$$F_{\rm d} = \dot{M}_{\rm acc}\,v_0 + \int_{2\xi_0}^{\infty} 2\pi\,v_0\,\bar{\rho}(\xi)\;(v_0 - v_\infty)\;\xi\,{\rm d}\xi. \quad (8)$$

The first term in the right-hand side is the drag caused by accretion of material and the second term is a purely gravitational drag by the material in the wake that will not be accreted. In order to obtain a closed expression for $F_{\rm d}$, it is convenient to introduce the new variables $l \equiv \xi/(2\xi_0)$, and $\lambda \equiv \xi_0/h$. With these variables and replacing Eqs. (4) and (6) into equation (8) the drag force can be written as:

$$F_{\rm d} = \dot{M}_{\rm acc}\,v_0 + 8\pi\rho_0\,v_0^2\,\xi_0^2\,\times \left\{\int_1^\infty {\rm e}^{-2\lambda^2\,l^2}{\rm I}_0\left(2\lambda^2\,l^2\right)\left[l - \left(l^2-1\right)^{1/2}\right]{\rm d}l\right\}. \quad (9)$$

The expressions for the mass accretion rate (equation 7), and for the gravitational drag (equation 9) are easy to compute numerically. Moreover, they can be further simplified in the limiting cases of a thin and thick disk, as shown below.

2.2. *Thick disk limit:* $\lambda \ll 1$

If the scaleheight of the disk is much larger than the gravitational radius (that is, $\lambda = (\xi_0/h) \ll 1$), the ${\rm I}_0$ Bessel function in equation (7) is close to unity, whereas the ${\rm I}_1$ is close to zero. After substituting ξ_0 by its definition in Equation (3), the accretion rate is approximately given by:

$$\dot{M}_{\rm acc,thick} \approx \frac{4\pi\,(G\,M)^2\,\rho_0}{v_0^3}\,, \quad (10)$$

which is the same expression obtained for the uniform density case (Cantó et al. 2011).

The mass accretion rate can be written in terms of the disk surface density given by

$$\Sigma = \int_{-\infty}^{\infty}\rho(y)\,{\rm d}y = \int_{-\infty}^{\infty}\rho_0\,{\rm e}^{-y^2/h^2}\,{\rm d}y = \sqrt{\pi}\,\rho_0\,h, \quad (11)$$

as :

$$\dot{M}_{\rm acc,thick} \approx \frac{4\sqrt{\pi}\,(G\,M)^2\,\Sigma}{h\,v_0^3}\,. \quad (12)$$

We may obtain an analytical expression for the drag force by using the following approximations

$${\rm e}^{-2\,\tau^2}\,{\rm I}_0\left(2\,\tau^2\right) \approx \quad 1 \quad ;\; 2\,\tau^2 \ll 1, \quad (13a)$$

$${\rm e}^{-2\,\tau^2}\,{\rm I}_{\rm n}\left(2\,\tau^2\right) \approx \tfrac{1}{2\,\sqrt{\pi}\,\tau}\;;\; 2\,\tau^2 \gg 1, \quad (13b)$$

to split the integral in equation (9) in two parts. A first integral over l in the range $1 < l < l_0$ (such that $2\lambda^2\,l^2 < 1$), and the second x-integral from x_0 to infinity (such that $2\lambda^2\,l^2 > 1$), where

$$l_0 = \frac{1}{2\sqrt{\pi}\,\lambda} \quad (14)$$

is the junction of the asymptotic expressions in Eqs. (13). More specifically,

$$\int_1^\infty {\rm e}^{-2\lambda^2\,l^2}{\rm I}_0\left(2\lambda^2\,l^2\right)\left[l - \left(l^2-1\right)^{1/2}\right]{\rm d}l \approx \int_1^{l_0}\left[l - \left(l^2-1\right)^{1/2}\right]{\rm d}l + \int_{l_0}^\infty \frac{l_0}{l}\left[l - \left(l^2-1\right)^{1/2}\right]{\rm d}l, \quad (15)$$

Performing the integrals, and using the accretion rate of equation (10), the total drag becomes

$$F_{\rm d,thick} \approx 4\pi\,\rho_0\,v_0^2\,\xi_0^2\left[-l_0^2 + l_0\sqrt{l_0^2-1} + 2\,l_0\,\arctan\left(\frac{1}{\sqrt{l_0^2-1}}\right) + \ln\left(l_0 + \sqrt{l_0^2-1}\right)\right]. \quad (16)$$

Remind that in terms of physical parameters, we have that $\xi_0^2 = (GM)^2/v_0^4$ and $l_0 = hv_0^2/(2\sqrt{\pi}GM)$. The associated Coulomb logarithm, defined as $\ln\Lambda = F_{\rm d}/(4\pi\rho_0\xi_0^2v_0^2)$, corresponds to the term in square brackets in Eq. (16). We see that the ambiguity in the definition of the minimum scale of interaction that appears in linear theory (e.g., Ostriker 1999 for the homogeneous medium, or Rein 2012 for the case of a disk), is removed in this approach. Moreover, no additional

cut-off scale needs to be introduced at large distances. Using the hydrodynamical approach in the linear regime, Rein (2012) identified a Coulomb logarithm but it is not the same as in the present work.

A yet simpler expression can be obtained taking the limit of $l_0 \gg 1$ (i.e. $\lambda \ll 1$; the thick disk limit) :

$$F_{\rm d,thick} \approx \frac{4\pi\,\rho_0\,(G\,M)^2}{v_0^2}\left[\frac{3}{2}+\ln\left(\frac{h}{\sqrt{\pi}\xi_0}\right)\right]. \qquad (17)$$

The error made by using the above expression instead of the exact formula (Eq. 9), is less than 2% for $\lambda \leq 0.5$. In terms of the disk surface density, the drag force in the thick disk approximation can be expressed as

$$F_{\rm d,thick} \approx \frac{4\sqrt{\pi}\,\Sigma\,(G\,M)^2}{v_0^2 h}\left[\ln\left(\frac{{\rm e}^{3/2}h}{\sqrt{\pi}\xi_0}\right)\right], \qquad (18)$$

where the factor ${\rm e}^{3/2}$ comes from inserting the term $3/2$ that appears in the right-hand side of Equation (17) in the argument of the logarithm.

For a homogeneous medium, Cantó et al. (2011) demonstrated that the drag force for hypersonic bodies can be written as

$$F_{\rm d} \approx \frac{4\pi\,\rho_0\,(G\,M)^2}{v_0^2}\ln\left(\frac{r_{\rm max}}{r_{\rm min}}\right), \qquad (19)$$

where $r_{\rm max}$ is the largest impact parameter and $r_{\rm min} = \sqrt{\rm e}\xi_0/2$. Comparing equations (18) and (19) we find that, in the case of a stratified medium, the ambiguity in the maximum impact parameter is removed. Adopting $r_{\rm min} = \sqrt{\rm e}\xi_0/2$ and using Eq. (18), we find $r_{\rm max} = {\rm e}^2 h/(2\sqrt{\pi}) \simeq 2.1h$ for a Gaussian disk. Hence, this implies that the gravitational drag on a supersonic body that is dropped suddenly at $t = 0$ in a stratified background, saturates asymptotically with time to a constant value. This also holds true if the disk is infinitesimally thin (see the next subsection and Muto et al. 2011).

2.3. *Thin disk limit:* $\lambda \gg 1$

For a thin disk ($h \ll \xi_0$, or $\lambda \gg 1$), one can use the approximation of equation (13a) in equation (7) to obtain the mass accretion rate:

$$\dot{M}_{\rm acc,thin} \approx 4\,\sqrt{\pi}\,\xi_0\,h\,\rho_0\,v_0, \qquad (20)$$

or in terms of the disk surface density (equation 11), after substitution of equation (3), as

$$\dot{M}_{\rm acc,thin} \approx 4\,\xi_0\,v_0\,\Sigma = \frac{4\,G\,M\,\Sigma}{v_0}. \qquad (21)$$

Notice that the accretion rate has a much weaker dependence on the velocity of the perturber v_0 than in the thick disk or uniform density cases (Equation 12), and that the dependence on the disk parameters is nicely folded into a single parameter (i.e., the surface density).

The net gravitational drag (including the drag due to accretion) on a body moving in a thin disk can be estimated combining equations (9, 13a, and 20), yielding :

$$F_{\rm d,thin} \approx 2\,\pi^{3/2}\,\rho_0\,v_0^2\,h\,\xi_0 = 2\,\pi\,G\,M\,\Sigma. \qquad (22)$$

Thus, the drag in a thin disk does not depend on v_0 (i.e., the relative velocity between the point mass and the surrounding environment), but solely on the surface density Σ of the disk and the mass M of the perturber. Furthermore, the gravitational deceleration on the hypersonic perturber $F_{\rm d}/M$ is independent of any of the parameters of the perturber (i.e. its mass or velocity) and depends, only, on the surface mass density of the disk.

It is common to compare the drag force in gaseous and collisionless media. Following Binney & Tremaine (1987), we have derived the dynamical friction force in a collisionless medium but, instead of assuming that the background particles are distributed homogeneously in a three-dimensional medium, we assume that they are distributed in the (x, z)-plane, i.e. two-dimensional geometry. We find that, if the perturber moves at a velocity much larger than the velocity dispersion of background particles, the dynamical friction is also given by Eq. (22). We must stress here that the structure of the wake and the underlying physics in gaseous media (where we may have gas accretion onto the perturber) and in collisionless media (no accretion occurs) are very different.

3. NUMERICAL SIMULATIONS

3.1. *The setup*

We have used the adaptive grid code YGUAZÚ-A (Raga et al. 2000) to perform a set of numerical simulations to be compared with the analytical model presented above. The version of the code employed solves the isothermal hydrodynamic equations on a three-dimensional Cartesian grid. The equations are solved with a second order implementation of the "flux vector splitting" algorithm of van Leer (1982).

We use the same reference system as that described in §2, in which the point mass is at rest at the center of the system. In units of ξ_0, the computational domain covers a region of $[(-7.5, 7.5), (0, 7.5), (-7.5, 7.5)]$, in x, y and z, respectively. The relevant scales that need to be solved are ξ_0 and h, the gravitational radius and the scaleheight of the disk, respectively. The domain is discretized in a five-level binary adaptive grid with a maximum resolution equivalent to $512 \times 256 \times 512$ cells in a uniform mesh. Simulations at half the resolution give similar results for the accretion rate and the drag, but with a smoother structure of the wake, due to numerical diffusion. The gravitational attraction due to a point mass centered at $(0, 0, 0)$ is added as an external source term. To avoid numerical artifacts a softening length of 10 cells is used for the gravitational force. The accretion onto the point mass is emulated by artificially keeping (at every timestep) a low density inside a hemisphere of radius $0.15\,\xi_0$ (~ 5 cells) centered around the point mass.

Different parameters have been used in the literature to measure the degree of non-linearity $\mathcal{A}$. In the case of the Bondi-Hoyle accretion problem, we will use $\mathcal{A} \equiv 2\xi_0/r_s$, which is the ratio between the accretion radius ($2\xi_0$) and the softening radius r_s. In our simulations $r_s = 0.3\xi_0$ and hence $\mathcal{A} \equiv 2\xi_0/r_s \simeq 6$. In astronomical systems, $\mathcal{A}$ may range between 1 and 100 for Earth-like and Jupiter-like planets, up to much higher values for black holes. However, a value of $\mathcal{A} \simeq 6$ is large enough to test the success of our analytical formalism in a situation in which non-linearity is important.

Since the problem has mirror symmetry on the $y = 0$ plane, we only simulate one half of the wake (for positive y), imposing a reflective boundary condition at $y = 0$. The subsequent analysis is done considering the mirror symmetry. The domain is initially filled with a streaming environment with a density given by the Gaussian profile of equation (1), and a constant velocity v_0 in the x direction. An inflow condition (with the appropriate density profile and velocity) is imposed on the $x = -7.5\xi_0$ boundary in order to replenish the streaming environment. Outflow conditions are imposed on the re-

TABLE 1
PARAMETERS OF THE SIMULATIONS[a].

Model	c_s	Mach number	$h\ [\xi_0]$	Regime
A	0.2	5	10^5	thick disk
B	0.2	5	2.0	thick disk
C	0.2	5	0.5	thin disk
D	0.1	10	0.5	thin disk

[a] In all models $\rho_0 = 1$, and $v_0 = 1.0$.

maining boundaries.

Because the flow is isothermal, the density gradient translates into a vertical pressure gradient that tends to destroy the disk, which is particularly problematic for the thin disk models (which have a larger pressure gradient). To avoid this we have added a vertical external force (in the $-y$ direction) that corresponds to the gravity force needed to maintain hydrostatic equilibrium. Additionally, to avoid numerical problems due to the large range of density values needed for the Gaussian profile, we have set a lower limit beyond a height of $y = 3\,\xi_0$. Past this height the density is homogeneous and the external vertical gravity is turned off. This has no noticeable consequences on the results as most of the mass and momentum lie closer to the midplane.

The parameters of the four models are summarized in Table 1. In all the models, we take units such that $\rho_0 = 1$ and $v_0 = 1$. The first two simulations (A and B) correspond to a thick disk. Given the large scaleheight used in model A, the ambient density is close to constant inside the domain, thus the model is basically a 3D version (albeit at a lower resolution due to computational constraints) of the simulation in Cantó et al. (2011). The other two models (C and D) correspond to a thin disk with the same scaleheight but different sound speeds. Models C and D have Mach numbers of 5 and 10, respectively. These two models were computed to test the result (of the analytic model) that the drag is independent of the Mach number of the flow.

3.2. *Results*

We allow the four models to run up to an evolutionary time of $t = 55\,\xi_0/v_0$, ensuring that a quasi-stationary state is achieved. Density maps for all the models after this integration time are displayed in Figure 2. In this figure we present a zoom of a region close to the point mass. The snapshots show the highly variable flow structure, formed downstream of the perturber centered at $(0, 0, 0)$.

In order to compare the numerical simulations with the free-streaming model, we have taken the density and velocity outputs and computed the mass flux (per unit of time) $\dot{M}$ and the net x-momentum flux, over cylinders of varying radii (ξ). More specifically,

$$\dot{M}(\xi) = \int_{S_\xi} \rho \boldsymbol{v} \cdot d\boldsymbol{S}, \tag{23}$$

$$F_{\rm D}(\xi) = \int_{S_\xi} \rho v_x \boldsymbol{v} \cdot d\boldsymbol{S}, \tag{24}$$

where S_ξ is the surface of a cylinder with axis along the x-axis, radius ξ and whose caps are placed at the boundaries of our domain, at $x = -7.5\xi_0$ and at $x = 7.5\xi_0$. In a steady state, $\dot{M}$ should not depend on ξ and must coincide with the accretion of mass onto the perturber $\dot{M}_{\rm acc}$. On the other hand, $F_{\rm D}(\xi)$ is the contribution of the mass inside a cylinder of radius ξ to the drag force. It includes both the force due to accretion of momentum over the body surface and the gravitational force on the perturber by its own wake. The drag force on the perturber $F_{\rm d}$ corresponds to $F_{\rm D}$ when all the mass in the wake is included, that is, in the limit $\xi \to \infty$. The results can be compared with the predictions of equations (10), (17), (21) and (22).

The results for $\dot{M}$ as a function of the cylindrical radius (i.e., the impact parameter) are presented in Figure 3. This figure gives the average $\dot{M}$ from $t = 51$ to 55, in units of ξ_0/v_0, with error bars denoting the maximum variability at each radius. The highly variable mass flux, sign of a very turbulent wake, evidenced by the large error bars, is consistent with previous calculations (see for instance Cantó et al. 2011). The solid line in the figures correspond to the asymptotic expressions for the thick (A, B) and thin (C, D) disk models, Equations (10) and (20), respectively. We have added the full solution for $\dot{M}$ (Equation 7), which is only appreciably different from the solid line in Figure 3(b). We can also see from Figure 3 that $\dot{M}$ becomes more or less independent of the impact parameter after $\xi = 2\,\xi_0$, the impact parameter beyond which the material remains unbound (see eq. 3).

It is also noticeable that there is a systematic difference towards smaller accretion rates compared to the analytical prediction. The reason for this offset is the limited length of the computational box. Material entering the downstream wake will travel a distance (see Cantó et al. 2011)

$$x_m = \frac{2\xi_0}{\left(2\xi_0/\xi\right)^2 - 1} \tag{25}$$

along the positive x-axis before turning around and falling towards the point mass. With the outflow boundary condition placed at $x = 7.5\,\xi_0$, all the mass that leaves the computational box is lost. From equation (25) we can see that only material with $\xi \lesssim 1.77\,\xi_0$ is captured, while all the mass with an impact parameter $\xi > 1.77\,\xi_0$ leaves the domain and does not contribute to the mass accretion. The effect of the limited domain size can be quantified by integrating the mass accretion (equation 5) only up to an impact parameter $1.77\,\xi_0$. The result is shown as a dashed line in the plots of Figure 3, agreeing well with the results from the simulations.

The flux $F_{\rm D}$ as a function of impact parameter (averaged over the same time window as the mass flux, see above) is presented in Figure 4. The gravitational drag in our simulations also shows a saturation for $\xi \geq 2\,\xi_0$, for all the models.

Comparing the two thin disk models in Figs. 4(c,d) we can see that indeed $F_{\rm d}$ is basically independent of the Mach number (provided that the flow is hypersonic).

The solid lines shown in Fig. 4 correspond to the analytical approximations given in equations (17) and (22), for the thick and thin disk models, respectively. We have also included the full solution of Equation (9) as a dotted line, which overlaps the solid lines except for model B. Since the net drag $F_{\rm d}$ has a term $\dot{M}_{\rm acc} v_0$ (see Eq. 9), we need to take into account that the accretion rate is slightly smaller than predicted by the model because of the limited extent of the computational box in the x-direction. Including this effect, a new corrected value is derived, which we display as a dashed line in Figure 4.

However, for model A, which has a scaleheight $h = 10^5\,\xi_0$, a direct application of equations (17) or (8) yields a drag force $F_{\rm d} \simeq 156\ \rho_0\, v_0^2\, \xi_0^2$, which is more than four times the computed value. The main reason for this discrepancy is that the

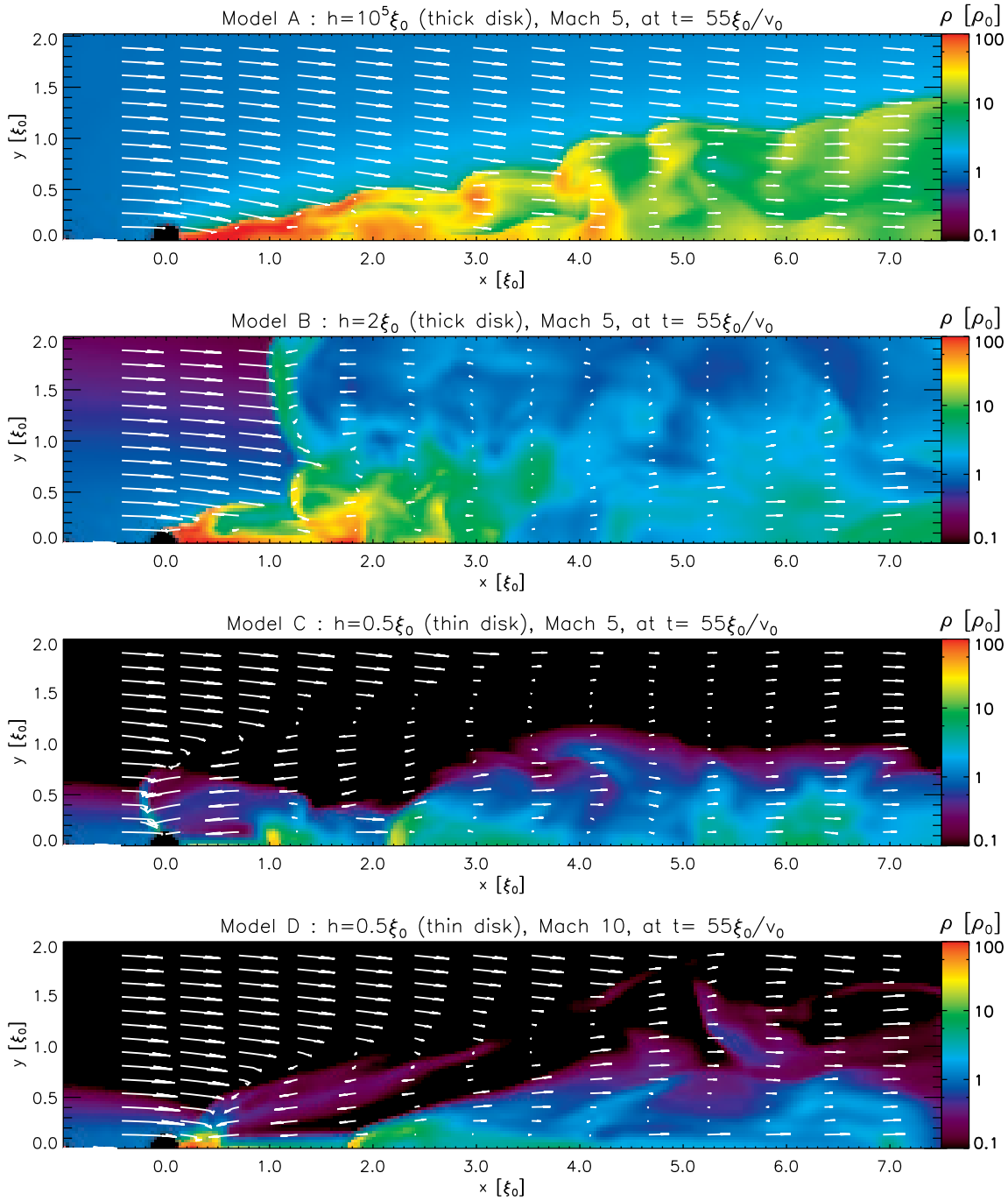

FIG. 2.— Cuts of density and velocity along the $z = 0$ plane after an integration time of $t = 55\xi_0/v_0$ for all the models (as indicated in the top labels). The gray-scale (color-scale in the online version) shows density, in units of the midplane density ρ_0, in logarithmic scale (as indicated by the bars on the right). The arrows represent the velocity field. The panels only show an inner region of the entire computational domain where the wake is formed. The perturber is located at $(0, 0)$ and the axes are given in units of ξ_0.

model considers all the mass in the disk, while the numerical simulation is restricted to the drag by streamlines with impact parameter less than $L_y = 7.5\xi_0$. In order to apply our analytical approach to our simulation (or to a truncated Gaussian disk), the integral in the right-hand side of Equation (9) should be performed between the lower limit $l = 1$ and the maximum impact parameter, in our case $l_{\rm max} = L_y/(2\xi_0) = 3.25$. For model A it results in a drag force $F_{\rm d} \simeq 27\,\rho_0\,v_0^2\xi_0^2$, which is the value plotted in Fig. 4(a) as a dashed line. For the remaining models B, C and D, this correction is marginal and the difference between the dashed, and the solid or dotted lines is due to the correction in the accretion rate.

In general we see that the agreement between the analytical model and the numerical values is good. The results for the higher Mach number model (D) agree slightly better, which is expected since the ballistic model is applicable to hypersonic flows.

4. DISCUSSION: APPLICABILITY OF THE MODEL TO A PLANET INSIDE A KEPLERIAN DISK

The models presented in this paper (analytical and numerical) consider a perturber traveling on a straight-line trajectory

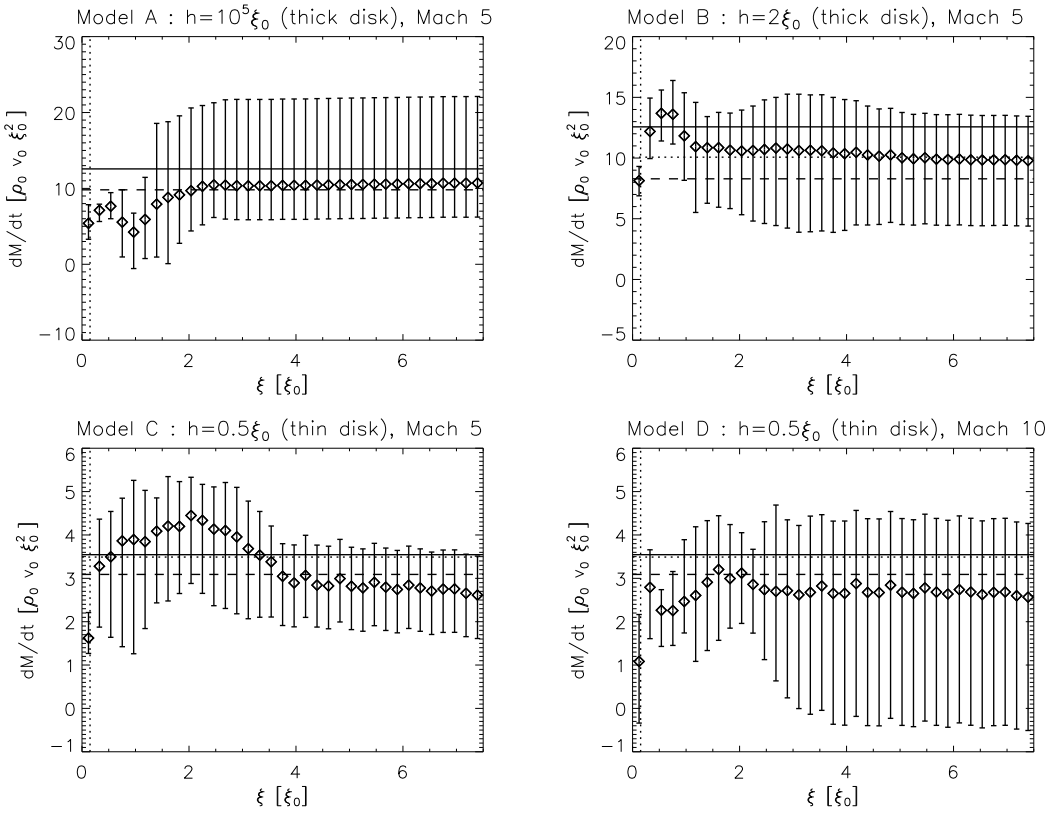

FIG. 3.— Mass flux $\dot{M}$ (in units of $\rho_0\, v_0\, \xi_0^2$) as a function of the cylindrical radius ξ of the control volume, in units of ξ_0. The symbols represent the average value (at each ξ) of the last five outputs in the simulations, corresponding to evolutionary times from 51 to $55\,\xi_0/v_0$. The error bars show the maximum departure from the mean value. The solid horizontal lines are the prediction from the analytical model: equation (10) for panels (a) and (b), and equation (20) for panels (c) and (d). The horizontal dotted line (overlaid with the solid line for A) shows the full solution from Eq. (7). The dashed horizontal lines show the full solution, but including a correction due to the limited extent of the computational box (see text for details). The vertical dotted lines depict the size of the perturber.

at constant velocity within a medium with a Gaussian density stratification. The medium has been regarded as a disk as one of the motivations was to obtain the drag force on an object orbiting in such a system (e.g. planets embedded in protoplanetary disks, or black holes in galactic nuclei). In a real situation, the perturbers move in complex orbits, the density of the disk and the relative velocity of perturber with respect to the ambient gas change with position, and the flow is not plane-parallel but presents differential rotation (shear). One can use the 'local' approximation, that is estimating the drag force at the present location of the perturber ignoring the curvature of the orbital motion, density gradients and shear effects, as long as the curvature radius is much larger than the scales involved in the model (i.e. ξ_0 and h).

The relevant scale for the drag force is h in the case of a gravitational perturber moving in a thick disk. Hence, since the relevant scale for curvature effects and shear is the size of the orbit, these effects can be ignored provided that the aspect ratio of the disk is small (see also Rein 2012).

In the following we consider the case of a thin disk. Let us consider the example of a planet in orbit inside a Keplerian disk to check under which conditions the model is adequate. A parcel of gas in a Keplerian disk around a star of mass M_* will have a velocity at a radius r_0 of [1] :

$$v_{\rm k} = \left(\frac{GM_*}{r_0}\right)^{1/2}. \tag{26}$$

The relative velocity between the planet in orbit with a velocity $\boldsymbol{v}_{\rm p}$ and the disk is $\boldsymbol{v}_0 = \boldsymbol{v}_{\rm p} - \boldsymbol{v}_{\rm k}$ and, therefore

$$v_0^2 = v_{\rm p}^2 + v_{\rm k}^2 - 2\boldsymbol{v}_{\rm p}\cdot\boldsymbol{v}_{\rm k} = v_{\rm k}^2\left(\alpha^2 + 1 - 2\alpha\cos p\right), \tag{27}$$

where

$$\alpha = \frac{v_{\rm p}}{v_{\rm k}}, \tag{28}$$

and p is the local pitch angle (the angle between $\boldsymbol{v}_p$ and the azimuthal direction). The planet is in corotation with the disk when $p = 0$ and $\alpha = 1$.

Combining equations (3), (26) and (27), we can write the ratio between the orbital radius and the planet gravitational radius as

$$\frac{r_0}{\xi_0} = \frac{M_*}{M_{\rm p}}\left(\alpha^2 + 1 - 2\alpha\cos p\right), \tag{29}$$

where $M_{\rm p}$ is the mass of the planet. Since the large-scale effects such as shear and curvature of both the orbit and the disk will be important when $r_0 \lesssim \xi_0$, we can use equation (29) to obtain the space of parameters α and p for which $\xi_0 < r_0$ and, hence, the local approximation is valid. This condition is

$$\frac{M_*}{M_{\rm p}}\left(\alpha^2 + 1 - 2\alpha\cos p\right) > 1. \tag{30}$$

We see that when p is close to $\pi/2$, the above condition is fulfilled for any value of α, provided that $M_* > M_p$. The most stringent condition for α occurs when $p \approx 0$, i.e. when the planet is close to pericenter and apocenter. Taking $p \approx 0$, we find that the condition (30) is not met for α's in the interval between α_- to α_+, where $\alpha_\pm \approx 1 \pm \sqrt{M_{\rm p}/M_*}$. If we take for

[1] This is only valid if there is no radial pressure gradient.

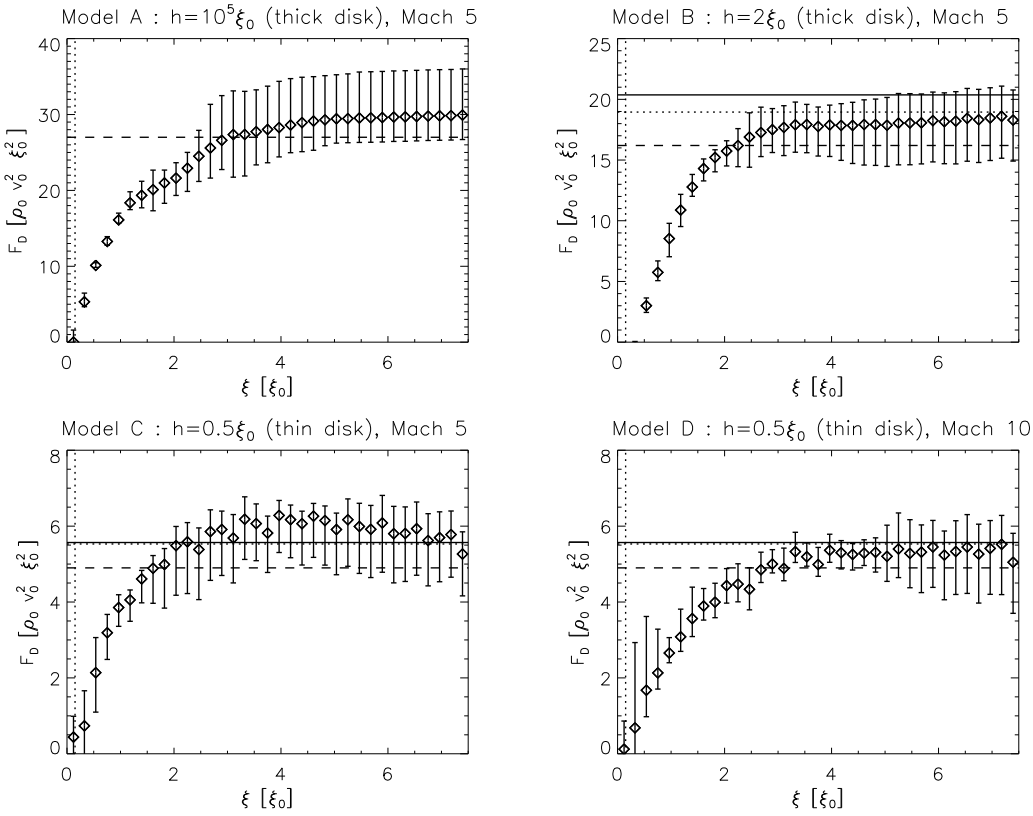

FIG. 4.— $F_{\rm D}$ (in units of $\rho_0\, v_0^2\, \xi_0^2$) as a function of the cylindrical radius ξ of the control volume, in units of ξ_0. For large values of ξ, it corresponds to the total drag onto the perturber. The symbols represent the average value (at each ξ) of the last five outputs in the simulations, corresponding to evolutionary times from 51 to $55\,\xi_0/v_0$, the error bars show the maximum departure from the value. The solid horizontal lines are the prediction from the analytical mode, equation (17) for A and B (For A the value is ~ 156, which lies outside the range plotted, see text for more details) and equation (22) for B and C. The horizontal dotted line (also ~ 156 for A) shows the full solution from Eq. (9). The dashed lines include the additional correction for the finite extent of the computational box, see text for details. The vertical dotted lines show the size of the perturber.

instance $M_*/M_{\rm p} = 1000$ (similar to the Sun/Jupiter system), it is simple to see that for orbits with eccentricities larger than 0.2, it holds that $\alpha > \alpha_+$ at pericenter, whereas $\alpha < \alpha_-$ at apocenter. Hence, we conclude that large-scale effects are small at any radius as long as $e > 0.2$.

A similar analysis can be done using the Hill radius of the planet in orbit :

$$r_{\rm H} \approx a\,(1-e)\left(\frac{M_{\rm p}}{3M_*}\right)^{1/3}, \qquad (31)$$

where a is the semi-major axis of the planetary orbit, and e its eccentricity. The Hill radius roughly defines the region around the planet in which its gravity dominates. Outside a sphere with radius $r_{\rm H}$ the gravitational pull from the central star is not negligible. Thus, in order to apply our model to the wake of a planet in a disk, the Hill radius has to be larger than a few times ξ_0 (the size of the wake). Replacing equation (29) into (31) we can write

$$\frac{r_{\rm H}}{\xi_0} = \frac{a\,(1-e)\left(\alpha^2+1-2\alpha\cos p\right)}{3^{1/3}\,r_0}\left(\frac{M_*}{M_{\rm p}}\right)^{2/3}. \qquad (32)$$

The gravitational pull from the star cannot be neglected if $r_{\rm H} \lesssim \xi_0$. Again, the stringest constraint for α occurs when $p \simeq 0$. In that case, the interval of α for which $r_{\rm H} < \xi_0$, is $\alpha'_- < \alpha < \alpha'_+$, where

$$\alpha'_\pm = 1 \pm 3^{1/6}\left[\frac{r_0}{a(1-e)}\right]^{1/2}\left(\frac{M_{\rm p}}{M_*}\right)^{1/3}. \qquad (33)$$

The factor in the square brackets in Eq. (33), that is $r_0/(a(1-e))$, varies between 1 at periastron to $(1+e)/(1-e)$ at apoastron. Let us consider the example of $M_*/M_{\rm p} = 1000$ in a highly eccentric orbit with $e = 0.8$. At the apoastron, we need $\alpha < \alpha'_- = 0.64$ to have $\xi_0 < r_{\rm H}$. This condition for α is fulfilled because $v_{\rm p}/v_{\rm k} = \sqrt{(1-e)/(1+e)}$ at apoastron. In general, $\xi_0 < r_{\rm H}$ at any radius of the orbit provided that $e > 0.2$. In conclusion, we have shown that, for eccentric orbits with $e > 0.2$ or retrograde disks, the curvature effects, as well as the pull from the central star, on the wake can be neglected.

5. SUMMARY

We present an analytical model for predicting the accretion rate and gravitational drag on a point mass that travels hypersonically along the midplane of a stratified medium with a Gaussian vertical density profile. The model considers that the trajectories of fluid parcels are ballistic, and is a direct extension of the uniform density case presented in Cantó et al. (2011). The analytic model was then compared with a set of three-dimensional, isothermal hydrodynamic simulations. In contrast to the geometry used in Cantó et al. (2011), in the present work cylindrical control volumes are used, which makes the treatment easier and more natural given the symmetry of the problem.

The results can be summarized as follows :

(i) Fully analytic expressions for the mass accretion rate $\dot{M}_{\rm acc}$ and the gravitational drag force $F_{\rm d}$ are obtained

assuming a free streaming ballistic flow.

(ii) Simpler expressions for $\dot{M}_{\rm acc}$ and $F_{\rm d}$ are obtained for two asymptotic limits; for a *thin disk*, in which the disk scaleheight is small compared to the gravitational radius, and for a *thick disk*, in which the disk scaleheight is large compared to the gravitational radius.

(iii) In a thick Gaussian atmosphere with vertical scaleheight h, and surface density Σ the drag force, including the contribution of the nonlinear part of the wake, is given by

$$F_{\rm d,thick} \approx \frac{4\sqrt{\pi}(GM)^2\Sigma}{h\,v_0^2}\ln\left(\frac{r_{\rm max}}{r_{\rm min}}\right)\,, \qquad (34)$$

where $r_{\rm min} = \sqrt{\rm e}GM/(2v_0^2)$ and $r_{\rm max} = {\rm e}^2h/(2\sqrt{\pi})$, while the mass accretion rate is

$$\dot{M}_{\rm acc,thick} \approx \frac{4\sqrt{\pi}(GM)^2\Sigma}{h\,v_0^3}\,. \qquad (35)$$

(iv) We find that the mass accretion onto a point mass M moving in a thin disk is proportional to M and to the surface density Σ of the disk,

$$\dot{M}_{\rm acc,thin} \approx \frac{4\,G\,M\,\Sigma}{v_0}\,. \qquad (36)$$

(v) The gravitational drag force in the *thin disk* regime is independent of the flow velocity (provided that the flow is hypersonic), and is also proportional to $M\Sigma$.

$$F_{\rm d,thin} \approx 2\,\pi\,G\,M\,\Sigma\,. \qquad (37)$$

At the same time the gravitational deceleration of the hypersonic perturber in a thin disk ($F_{\rm d}/M$) is independent of its parameters (i.e. mass or velocity) and depends only on the surface mass density of the disk.

(vi) The mass accretion in the simulations was highly variable. The analytic prediction is slightly higher than the average values obtained from the simulations, but well within their dispersion. These differences might be due to the relatively low resolution of our present three-dimensional simulations.

(vii) The drag force computed from the simulations showed a good agreement with the analytic model, with a lower dispersion compared with the accretion rates. The result (from the analytic model) that, in a thin disk, the drag force is independent of the Mach number of the flow is confirmed by the numerical simulations.

The referee is deeply thanked for an exhaustive scrutiny of the manuscript. This work has been supported by CONACYT grants 61547, 101356, 101975, 165584 and 167611, as well as DGAPA-UNAM IN105312 and IN106212 grants.

REFERENCES

Begelman, M. C., Blandford, R. D., Rees, M. J. 1980, Nature, 287, 307
Binney, J. 1977, MNRAS, 181, 735
Binney, J. & Tremaine, S. 1987, Galactic Dynamics, Princeton University Press (Princeton, New Jersey)
Bisnovatyi-Kogan, G. S., Kazhdan, Y. M., Klypin, A. A., Lutskii, A. E., & Shakura, N. I. 1979, Soviet Ast., 23, 201
Bondi, H. 1952, MNRAS, 112, 195
Bondi, H., Hoyle, F. 1944, MNRAS, 104, 273
Bonnell, I. A., Bate, M. R., Clarke, C. J., Pringle, J. E. 2001a, MNRAS, 323, 785
Bonnell, I. A., Clarke, C. J., Bate, M. R., Pringle, J. E. 2001b, MNRAS, 324, 573
Cantó, J., Raga, A. C., Esquivel, A., & Sánchez-Salcedo, F. J. 2011, MNRAS, 418, 1238
Colpi, M., Mayer, L., Governato, F. 1999, ApJ, 525, 720
Cuadra, J., Armitage, P. J., Alexander, R. D., Begelman, M. C. 2009, MNRAS, 393, 1423
Di Matteo, T., Carilli, C. L., Fabian, A. C. 2001, ApJ, 547, 131
Dokuchaev, V. P. 1964, Soviet Astron., 8, 23
Dotti M., Volonteri M., Perego A., Colpi M., Ruszkowski M., Haardt F. 2010, MNRAS, 402, 682
Escala, A., Larson, R. B., Coppi, P. S., Mardones, D. 2005, ApJ, 630, 152
Hoyle, F., & Lyttleton R. A. 1939, Proc. Cambridge Philos. Soc., 35, 405
Hoyle, F., & Lyttleton R. A. 1940a, Proc. Cambridge Philos. Soc., 36, 323
Hoyle, F., & Lyttleton R. A. 1940b, Proc. Cambridge Philos. Soc., 36, 325
Hoyle, F., & Lyttleton R. A. 1940c, Proc. Cambridge Philos. Soc., 36, 424
Just, A., Kegel, W. H. 1990, A&A, 232, 447
Just, A., Peñarrubia, J. 2005, A&A, 431, 861
Khan, F. M., Just, A., Merritt, D. 2011, ApJ, 732, 89
Kim, H., Kim, W.-T. 2007, ApJ, 665, 432
Klessen, R. S., Burkert, A. 2000, ApJS, 128, 287
Klessen, R. S., Burkert, A. 2000, ApJ, 549, 386
Maoz E. 1993, MNRAS, 263, 75
Muto, T., Takeuchi, T., Ida, S. 2011, ApJ, 737, 37
Namouni, F. 2010, MNRAS, 401, 319
Nixon, C. J., Cossins, P. J., King, A. R., Pringle, J. E. 2011a, MNRAS, 412, 1591
Nixon, C. J., King, A. R., Pringle, J. E. 2011b, MNRAS, 417, L66
Preto, M., Berentzen, I., Berczik, P., Spurzem R. 2011, ApJ, 732, L26
Raga, A. C., Navarro-González, R., & Villagrán-Muniz, M. 2000, Revista Mexicana de Astronomia y Astrofisica, 36, 67
Rein, H. 2012, MNRAS, 422, 3611
Roedig, C., Sesana, A. Dotti, M., Cuadra, J., Amaro-Seoane, P., Haardt, F. 2012, arXiv:1202.6063
Ruderman, M. A., Spiegel, E. A. 1971, ApJ, 165, 1
Sánchez-Salcedo, F. J. 2009, MNRAS, 392, 1573
Sánchez-Salcedo, F. J. 2012, ApJ, 745, 135
Sánchez-Salcedo, F. J., Brandenburg, A. 2001, MNRAS, 322, 67
Tanaka, T., Haiman, Z. 2009, ApJ, 696, 1798
Tremaine, S., Weinberg, M. D. 1984, MNRAS, 209, 729
van Leer, B. 1982, in Lecture Notes in Physics, Berlin Springer Verlag, Vol. 170, Numerical Methods in Fluid Dynamics, ed. E. Krause, 507–512